Spectrally selective infrared absorption in defect-mode photonic-crystal-slab cavity

Weidong Zhou,[a] Li Chen,[a] Zexuan Qiang,[a] and Gail J. Brown[b]
[a] Department of Electrical Engineering, NanoFAB Center, University of Texas at Arlington, TX 76019, USA
wzhou@uta.edu
[b] Air Force Research Laboratory, Materials & Manufacturing Directorate, Wright Patterson AFB, OH 45433-7707, USA
Gail.Brown@wpafb.af.mil

Abstract. Significantly enhanced absorption at the defect mode can be obtained at surface-normal direction in a dielectric single-defect photonic-crystal-slab, with an absorption enhancement factor greater than 4,000. Complete absorption suppression within the photonic bandgap region can also be observed in defect-free photonic crystal cavities. High spectral selectivity and tunability is feasible with defect mode engineering, making photonic crystal defect cavities a promising nanophotonic platform for the spectrally selective infrared sensing and hyper-spectral imaging, with the incorporation of quantum well or quantum dot infrared photodetector heterostructures.

Keywords: photonic-crystal-slabs, defect-mode cavity, infrared absorption.

1 INTRODUCTION

Photonic crystal (PC) exhibits photonic band gaps (PBGs) and unconventional dispersion and refractive properties making possible hitherto not realizable optical devices such as ultra-compact routers, highly wavelength selective and compact add/drop filters [1, 2]. Owing to the ability of spontaneous emission control [1, 3], photonic crystal slab (PCS) [4] waveguide cavities have been a subject of active research for ultra-compact high efficiency light sources [5, 6], with potentially zero threshold [7-10]. Additionally, PC structures can lead to other physical phenomena, e.g., optical absorption property alteration, through the photonic density of states (DOS) engineering [11]. Enhancement and suppression of thermal emission and absorption reported so far are mostly based on bandedge effect in various metallic PC structures or clusters. Enhanced absorption can happen near or at the band edge where the electromagnetic Bloch wave is still extended throughout the structure, its group velocity is near zero, and the photonic DOS is greatly increased. In this regime, enhanced light-matter interaction is expected, and enhanced laser gain, light absorption and nonlinear effects have all been proposed [2, 11-17]. Enhanced absorption in tungsten 3D PCs has been reported [18]. Both theoretical and experimental research has been carried out and confirmed the modification of the Planck blackbody radiation [19]. Most of the work so far has been focused on the absorption change in one-dimensional distributed Bragg reflector (1D DBR) based cavities [12, 20], or one-, two- and three-dimensional (1D, 2D, 3D) metallic photonic crystal cavities [11, 13, 17]. Little work has been reported on the modified *absorption* characteristics in 2D *dielectric* photonic crystal slab (PCS) cavities [14], to the best of our knowledge.

Simultaneous inhibition and redistribution of spontaneous emission in PC has been demonstrated theoretically and experimentally in a lossless dielectric PCS structure [3]. The introduction of an absorption layer in a dielectric PCS structure (e.g. quantum well, quantum dots) can lead to the modification of the absorption characteristics, due to the spectrally-selective light-matter interaction in the cavity. We propose a photonic crystal infrared

Received 17 Apr 2007; accepted 22 Jun 2007; published 26 Jun 2007 [CCC: 19342608/2007/$25.00]

photodetector (PCIP) configuration, where the photonic crystal defect cavity was integrated with the quantum dot infrared photodetectors (QDIPs) [14, 21] for higher operation temperature and spectrally selective absorption, highly desirable for infrared gas sensing and hyper-spectral imaging. High spectral selectivity with tunable wavelength coverage and spectral width can be feasible based on defect engineering and simple lithographic control, and/or external control [22].

2 ABSORBTIVE PHOTONIC CRYSTAL SLAB SIMULATION

Following a similar approach reported by Fujita *et. al.* [3], three-dimensional (3D) finite-difference time-domain (FDTD) [23] simulation was carried out in a triangular lattice air hole PC cavity, with an absorptive layer in the center of the symmetric air-slab-air PCS, as shown in Fig. 1a. The structural parameters are also shown, along with the simulated photonic bandgap (PBG) and the defect mode characteristics in the single defect (H1) air hole photonic crystal slab (PCS) cavity with lattice constant a = 0.38μm. The defect level was confirmed to be a dipole mode (top inset of Fig. 1a) with center wavelength (1.504 μm) close to the center of the photonic bandgap (1.41 to 1.67μm). The absorption layer extinction coefficient k_a, i.e., the imaginary part of the refractive index, was tuned for different absorption coefficient α ($k_a = \alpha\lambda/(4\pi)$).

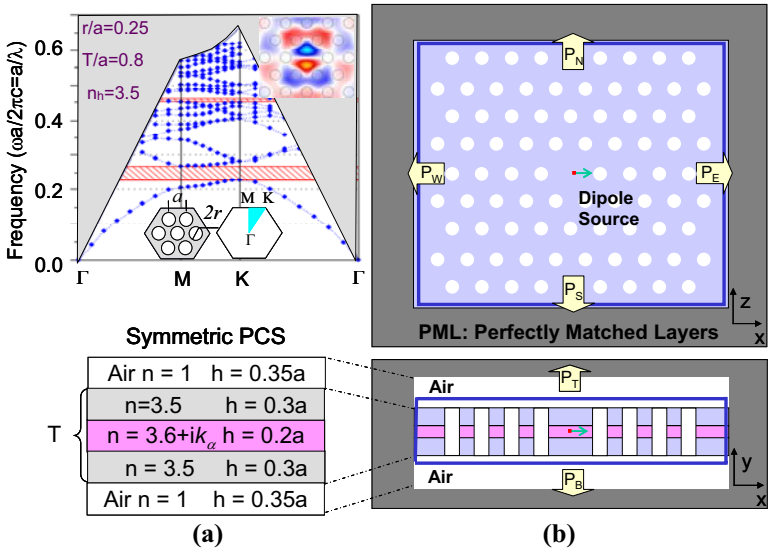

Fig. 1 (a) Photonic bandgap dispersion plot for the symmetric air-slab-air photonic crystal slab, with the thin absorptive layer inserted in the center of the slab, where the dispersion plot was simulated assuming $k_a = 0$. The dipole mode profile was also shown as the top inset for the single defect cavity at resonant wavelength of 1.504μm with lattice constant a = 0.38μm. (b) 3D FDTD simulation setup with perfectly matched layers as the boundary. An in-plane dipole source was placed at the center of the slab (red square dot) with monitors (blue lines) surrounding the simulation domain for both vertical and in-plane power monitoring.

Perfectly matched layers (PMLs) were incorporated at the boundaries of the computational domain to avoid unnecessary reflections of light at the boundaries. Typically the PMLs should be set about half wavelength away from the structure under simulation in order to separate the vertical and in-plane components (e.g., for the quality factor calculations). In our case, by placing monitors close to the dielectric slab structure, we see

little change in the total power monitored for each monitors when the thickness of the air section shown in Fig. 1a and 1b) changed from 2a (~half wavelength) to 0.35a, where a is the lattice constant. To save the computational resources (memory and time), we focused our work here with air region set to be 0.35a. A dipole source was introduced in the center of the cavity launching to the +x direction, with a Gaussian profile to cover the desired wavelength region of interest. Total of six power monitors were placed at the boundaries to collect the transmitted spectral power density after Fourier-transformation from the average of the Poynting vectors, for both in-plane power change (labeled as east (P_E), west (P_W), north (P_N) and south (P_S), respectively, as shown in Fig. 1b), and vertical power change (top (P_T) and bottom (P_B)). The same simulation was performed for the slab waveguide without photonic crystals as the reference. The absorption results were normalized to the one obtained from the reference sample (slab without PC).

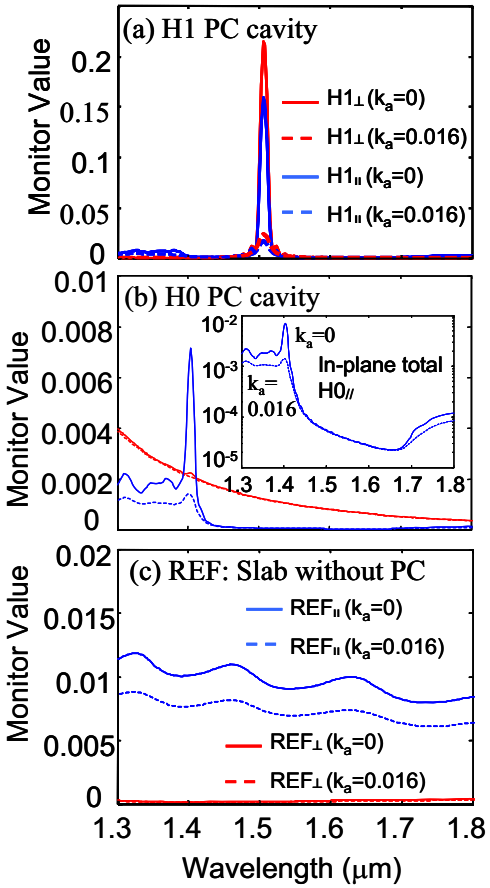

Fig. 2. Spectral power density based on the vertical and in-plane monitors in (a) single defect H1 PC cavity; (b) defect-free H0 PC cavity; and (c) reference slab without PC structure. To show the fine spectral features and relative transmitted power spectra density, the log-scale plot was inserted in (b), where bandgap suppression was shown along with an absorption peak at the bandedge.

The monitor power (transmitted spectral density) was shown in Fig. 2, with k_a = 0.016 (corresponding absorption coefficient α value of 1340 cm^{-1} at wavelength λ = 1500 nm), in three different cavities: (a) single defect H1 cavity; (b) defect-free H0 cavity; and (c) a conventional slab structure without photonic crystals (reference, slab w/o PC). It is evident that a significantly enhanced transmission at the defect level was obtained, mainly in the vertical direction. Reduced transmission with the incorporation of an absorption layer was

also seen in Fig. 2. It is worth mentioning that the dominant transmission at defect level is along vertical direction, due to the coupling of guided resonant cavity mode to the vertical leaky/radiation mode [24]. On the other hand, in the defect-free PC cavity (H0, inset of Fig. 2b), there is a significant suppression in the transmitted power within the photonic bandgap (PBG) region. At a much reduced signal level (transmitted power), there is a peak near the bandedge (1.41μm). This could be due to the bandedge effect associated with the group velocity anomaly. The transmitted power for the reference sample (no PC case) is also shown in Fig. 2c.

The absorption power was extracted from the monitored power difference at different absorption coefficients (varying k_a values). The normalized absorption, defined to be the ratio of the absorption in PC cavities to that value in reference slab without PC structures, were plotted in Fig. 3, with both linear (top) and log-scale (bottom), for single defect (H1) and defect-free (H0) PC cavities. Note only the absorption in the vertical direction was shown since the dominant absorption occurs in the vertical (surface normal) direction, as compared to the in-plane absorption. While absorption suppression is evident inside the PBG region, the enhanced absorption is seen at the defect level within the bandgap.

It is also worth mentioning that the defect mode quality factor Q is far from optimal. Defect mode cavity Q optimization [25, 26] is essential with much higher Q for the desired spectral selectivity for hyper-spectral imaging, or even ultra-spectral (0.1-0.3cm^{-1} resolution) imaging applications.

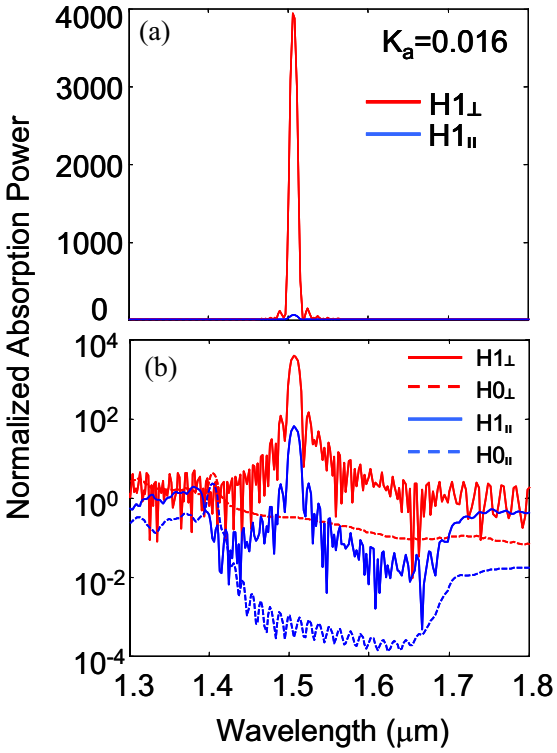

Fig. 3. (a) Linear and (b) Log-scale plot of normalized absorption power spectra with respect to the reference sample (slab without PC) for k_a= 0.016. Both vertical component (H1⊥, H0⊥) and in-plane component (H1$_{//}$, H0$_{//}$) were shown separately.

The absorption enhancement factor, defined as the relative absorption power spectral density compared to that obtained from the reference slab (without PC) with the same absorption coefficient, can be derived from the normalized absorption power spectral density

at the wavelength of interest. The absorption change (absorption enhancement factor) due to the presence of the PC cavity is shown in Fig. 4a, at the defect-level wavelength (1.5 μm), for different absorption coefficients. Enhanced absorption can be obtained with the enhancement factor around 6,000 with $k_a = 0.008$ (or $\alpha = 670$ cm^{-1}). The high enhancement factor (>1,000) can be obtained for a large range of absorption coefficients. The effect of air hole period surrounding the defect cavity was also investigated. With the reduction in the air hole period surrounding the single defect cavity from 4 to 3 periods, the enhancement factor also reduces accordingly by a factor of 10 for vertical absorption in H1 cavity, due to the corresponding reduction in the cavity quality factor Q (from 107 to 88). Shown in Fig. 4b is the total cavity quality factor Q for this single defect cavity mode, which is derived from the simulated defect mode linewidth (e.g. Fig. 2a), using equation $Q = \lambda/\delta\lambda$, where λ and $\delta\lambda$ are the center resonant wavelength and the corresponding linewidth, respectively. A reduction in Q was seen, as a result of increased absorption coefficient. Note the total Q relates to the in-plane $Q_{//}$ and vertical $Q_{\perp}$.with this equation: $Q^{-1} = Q_{//}^{-1} + Q_{\perp}^{-1}$. Similar values were obtained for the total cavity Q based on both vertical and in-plane defect mode linewidths ($H1_{\perp}$, $H1_{//}$). It is also anticipated that much higher Q can be achieved with higher enhancement factor by increasing the surrounding air hole period and defect engineering (increasing $Q_{//}$), and/or heterostructure slab engineering for optical vertical confinement (increasing $Q_{\perp}$) [25, 26].

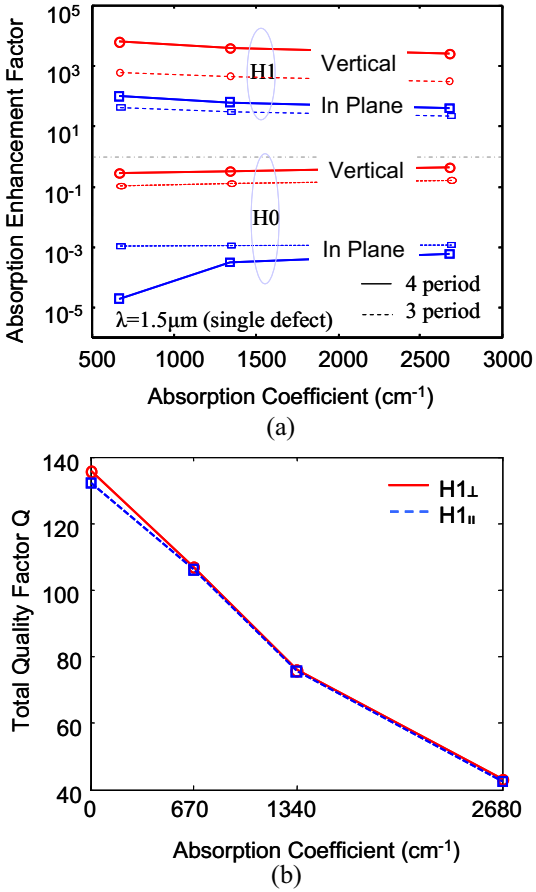

Fig. 4. (a) Absorption enhancement factor for H1 and H0 cavity for different absorption coefficients and different surrounding air hole periods (4 and 3 periods). Note the dominant absorption occurs along the vertical (top) direction. (b) Total quality factor Q for the single defect cavity H1 ($H1_{\perp}$, $H1_{//}$) at different absorption coefficients.

CONCLUSION

In conclusion, theoretical investigation has been carried out on the spectrally selective absorption properties in 2D dielectric PCS cavities, for the first time. The work is based on 3D FDTD technique. For 2D symmetric air hole triangular lattice PCS structures, enhanced absorption at defect level was obtained, with the enhancement factor greater than 4,000. Complete absorption suppression within photonic bandgap region was observed in defect-free cavities. The findings here can aid the cavity design in the infrared (IR) photodetectors with the incorporation of PC cavities. The incorporation of PC into IR photodetectors (e.g. quantum well and quantum dot infrared photodetectors at mid-wave, long-wave to far-infrared) can potentially lead to IR photodetectors with higher operation temperature due to enhanced spectrally selective absorption. The spectral resolution and tunability can be accomplished by controlling the cavity Q and resonant peak locations through PC defect engineering. The exact enhancement factor will be largely depending on cavity characteristics and the absorption coefficient at different IR bands. Similar results can also be obtained with surface normal incident light, via the coupling between in-plane guided resonance and vertical radiation modes [24].

Acknowledgments

The authors acknowledge the helpful discussions with Dr. M. Lu. This work was supported by Air Force Office of Scientific Research, and by National Science Foundation.

References

[1] E. Yablonovitch, "Inhibited spontaneous emission in solid-state physics and electronics," *Phys. Rev. Lett.* **58**(20), 2059-2062 (1987) [doi:10.1103/PhysRevLett.58.2059].

[2] S. Noda and T. Baba, *Roadmap on Photonic Crystals*, Springer, Heidelberg, Germany (2003).

[3] M. Fujita, S. Takahashi, Y. Tanaka, T. Asano, and S. Noda, "Simultaneous inhibition and redistribution of spontaneous light emission in photonic crystals," *Science* **308**, 1296-1298 (2005) [doi:10.1126/science.1110417].

[4] S. G. Johnson, S. Fan, P. R. Villeneuve, J. D. Joannopoulos, and L. A. Kolodziejski, "Guided modes in photonic crystal slabs," *Phys. Rev. B* **60**(8), 5751-5758 (1999) [doi:10.1103/PhysRevB.60.5751].

[5] O. Painter, R. K. Lee, A. Scherer, A. Yariv, J. D. O'Brien, P. D. Dapkus, and I. Kim, "Two-dimensional photonic band-gap defect mode laser," *Science* **284,** 1819-1821 (1999).

[6] J. K. Hwang, H. Y. Ryu, D. S. Song, I. Y. Han, H. K. Park, D. H. Jang, and Y. H. Lee, "Continuous room-temperature operation of optically pumped two-dimensional photonic crystal lasers at 1.6 um," *IEEE Photon. Technol. Lett.* **12**(10), 1295-1297 (2000) [doi:10.1109/68.883808].

[7] W. D. Zhou, J. Sabarinathan, P. Bhattacharya, B. Kochman, E. W. Berg, P. C. Yu, and S. W. Pang, "Characteristics of a photonic bandgap single defect micro-cavity electroluminescent device," *IEEE J. Quantum. Electron.* **37**(9), 1153-1160 (2001) [doi:10.1109/3.945320].

[8] R. Colombelli, K. Srinivasan, M. Troccoli, O. Painter, C. F. Gmachl, D. M. Tennant, A. M. Sergent, D. L. Sivco, A. Y. Cho, and F. Capasso, "Quantum cascade surface-emitting photonic crystal laser," *Science* **302**(5649), 1374-1377 (2003) [doi:10.1126/science.1090561].

[9] H. G. Park, S. H. Kim, S. H. Kwon, Y. G. Ju, J. K. Yang, J. H. Baek, S. B. Kim, and Y. H. Lee, "Electrically driven single-cell photonic crystal laser," *Science* **305**(5689), 1444-1447 (2004) [doi:10.1126/science.1100968].

[10] H. Altug and J. Vuckovic, "Photonic crystal nanocavity array laser," *Opt. Exp.* **13**(22), 8819-8828 (2005) [doi:10.1364/OPEX.13.008819].

[11] S. Y. Lin, J. G. Fleming, Z. Y. Li, I. El-Kady, R. Biswas, and K. M. Ho, "Origin of absorption enhancement in a tungsten, three-dimensional photonic crystal," *J. Opt. Soc. Am. B* **20**(7), 1538-1541 (2003).

[12] Y. Xi, X. Wang, X. Hu, X. Liu, and J. Zi, "Modification of absorption of a bulk material by photonic crystals," *Chin. Phys. Lett.* **19,** 1819-1821 (2002) [doi:10.1088/0256-307X/19/12/323].

[13] J. Yu, Y. Shen, X. Liu, R. Fu, J. Zi, and Z. Zhu, "Absorption in one-dimensional metallic-dielectric photonic crystals," *J. Phys.: Condens. Matter* **16**(7), L51-56 (2004) [doi: 10.1088/0953-8984/16/7/L01].

[14] K. T. Posani, V. Tripathi, S. Annamalai, N. R. Weisse-Bernstein, S. Krishna, R. Perahia, O. Crisafulli, and O. J. Painter, "Nanoscale quantum dot infrared sensors with photonic crystal cavity," *Appl. Phys. Lett.* **88,** 151104 (2006) [doi:10.1063/1.2194167].

[15] B. Temelkuran, E. Ozbay, J. P. Kavanaugh, G. Tuttle, and K. M. Ho, "Resonant cavity enhanced detectors embedded in photonic crystals," *Appl. Phys. Lett.* **72**(19), 2376-2378 (1998) [doi:10.1063/1.121361].

[16] M. Florescu, H. Lee, A. J. Stimpson, and J. Dowling, "Thermal emission and absorption of radiation in finite inverted-opal photonic crystals," *Phys. Rev. A* **72,** 033821 (2005) [doi:10.1103/PhysRevA.72.033821].

[17] G. Veronis, R. W. Dutton, and S. Fan, "Metallic photonic crystals with strong broadband absorption at optical frequencies over wide angular range," *J. Appl. Phys.* **97**, 093104 (2005) [doi:10.1063/1.1889248].

[18] J. G. Fleming, S. Y. Lin, I. El-Kady, R. Biswas, and K. M. Ho, "All-metallic three-dimensional photonic crystals with a large infrared bandgap," *Nature* **417**, 52-55 (2002) [doi:10.1063/1.1889248].

[19] S. Y. Lin, J. Moreno, and J. G. Fleming, "Three-dimensional photonic-crystal emitter for thermal photovoltaic power generation," *Appl. Phys. Lett.* **83**(2), 380-382 (2003) [doi:10.1063/1.1592614].

[20] M. S. Unlu and S. Strite, "Resonant cavity enhanced photonic devices," *J. Appl. Phys.* **78**(2), 607-639 (1995) [doi:10.1063/1.360322].

[21] P. Bhattacharya, S. Ghosh, and A. D. Stiff-Roberts, "Quantum dot opto-electronic devices," *Annu. Rev. Mater. Res.* **34**, 1-40 (2004) [doi:10.1146/annurev.matsci.34.040203.111535].

[22] O. Painter, A. Husain, A. Scherer, P. T. Lee, I. Kim, J. D. O'Brien, and P. D. Dapkus, "Lithographic tuning of a two-dimensional photonic crystal laser array," *IEEE Photon. Technol. Lett.* **12**(9), 1126-1128 (2000) [doi: 10.1109/68.874210].

[23] A. Taflove, *Computational Electrodynamics: The Finite-Difference Time-Domain Method,* Artech House, Boston, (1995).

[24] S. Fan and J. D. Joannopoulos, "Analysis of guided resonances in photonic crystal slabs," *Phys. Rev. B* **65**(23), 235112 (2002) [doi:10.1103/PhysRevB.65.235112].

[25] B. S. Song, S. Noda, T. Asano, and Y. Akahane, "Ultra-high-Q photonic double-heterostructure nanocavity," *Nature Mat.* **4**, 207-210 (2005) [doi:10.1038/nmat1320].

[26] E. Kuramochi, M. Notomi, S. Mitsugi, A. Shinya, and T. Tanabe, "Ultrahigh-Q photonic crystal nanocavities realized by the local width modulation of a line defect," *Appl. Phys. Lett.* **88**, 041112 (2006) [doi:10.1063/1.2167801].